ACS APPLIED MATERIALS & INTERFACES

Research Article

www.acsami.org

Competitive Adsorption of Dopamine and Rhodamine 6G on the Surface of Graphene Oxide

Hui Ren,[†,§,‡] Dhaval D. Kulkarni,[†,‡] Rajesh Kodiyath,[†] Weinan Xu,[†] Ikjun Choi,[†] and Vladimir V. Tsukruk*[,†]

[†]School of Materials Science and Engineering, Georgia Institute of Technology, Atlanta, Georgia 30332-0245, United States

[§]Key Laboratory of Explosion Science and Technology, School of Mechanoelectronic Engineering, Beijing Institute of Technology, Beijing 100081, P.R.C.

ABSTRACT: Competitive adsorption−desorption behavior of popular fluorescent labeling and bioanalyte molecules, Rhodamine 6G (R6G) and dopamine (DA), on a chemically heterogeneous graphene oxide (GO) surface is discussed in this study. Individually, R6G and DA compounds were found to adsorb rapidly on the surface of graphene oxide as they followed the traditional Langmuir adsorption behavior. FTIR analysis suggested that both R6G and DA molecules predominantly adsorb on the hydrophilic oxidized regions of the GO surface. Thus, when R6G and DA compounds were adsorbed from mixed solution, competitive adsorption was observed around the oxygen-containing groups of GO sheets, which resulted in partial desorption of R6G molecules from the surface of GO into the solution. The desorbed R6G molecules can be monitored by fluorescence change in solution and was dependent on the DA concentration. We suggest that the efficient competitive adsorption of different strongly bound bioanalytes onto GO−dye complex can be used for the development of sensitive and selective colorimetric biosensors.

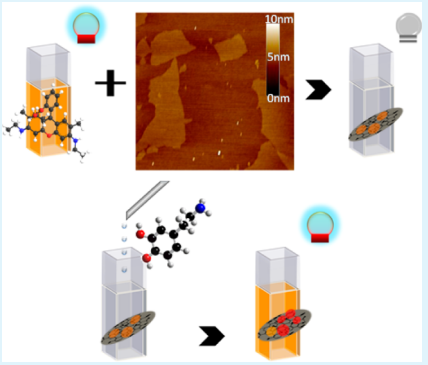

KEYWORDS: *competitive adsorption, graphene oxide, dopamine, Rhodamine 6G, fluorescence*

INTRODUCTION

Carbon-based nanomaterials have been studied as superior adsorbents in aqueous solutions for their potential environmental applications to isolate chemicals and pollutants,[1] such as organic pollutants[2] and metals[3] with high capacity and selectivity. One of the advantages of carbon-based nanoparticles as attractive adsorbents is that they have much larger specific surface areas than many other materials. Specific surface areas for activated carbon, porous carbon, and carbon nanotubes were estimated to be between 700 and 1600 m^2/g,[4−6] whereas single grapheme sheets revealed a much higher specific surface area up to 2630 m^2/g.[7]

Recent developments in the use of graphene oxide (GO), another carbon-based material with high surface activity, have showed immense promise in its application for separation and detection of trace levels of organic and inorganic analytes.[8−10] Rich oxygen-containing groups, such as −COOH, −CO, and −OH are known to occupy up to 60% of the graphene oxide surface area.[11] These are the essential chemical skeletons for an ideal highly porous adsorbent, as they can be used as anchoring sites, potentially making graphene oxide a more efficient adsorbent as well as a highly surface active functional filler.[12−15] Compared to other carbon nanomaterials, the important advantage of GO is its good water-solubility, versatile surface modification, and fluorescence quenching property all important for sensing of complex molecules such as bioanalytes.

In fact, Xu et al. indicated that the Brunauer−Emmett−Teller (BET)surface area of graphene oxide was 332 m^2/g, and after reduction with hydrazine, it increased to 617 m^2/g.[16] Stankovich et al. prepared graphene-based sheets via chemical reduction of exfoliated GO.[17] The surface area measurement of the reduced GO sheets via nitrogen gas absorption yielded a BET value of 466 m^2/g. Park et al. synthesized chemically reduced GO and measured a surface area of 487 m^2/g by the BET method.[18] Although the BET surface area of GO is lower than that of graphene, graphene oxide has abundant oxygen-containing surface groups, is inexpensive, and is readily dispersed in an aqueous environment.

The structure of graphene oxide sheets has been debated with uncertainty pertaining to both the type and distribution of oxygen-containing functional groups and surface charges.[19−22] It is generally suggested that GO possesses various oxygenated functionalities such as hydroxyl and epoxy on the basal plane and carboxyl group at the edges (Figure 1).[23] The surface of GO is highly heterogeneous with both hydrophobic pristine graphene regions and hydrophilic oxidized areas.[24,25] Due to its specific surface structure, it interacts strongly with organic, polymeric, and biological molecules, via noncovalent forces, such as hydrogen bonding, $\pi-\pi$ stacking, electrostatic forces, van der Waals forces, and hydrophobic interactions.

Indeed, it has been reported that graphene oxide shows excellent adsorption capacity for the removal of heavy metal

Received: November 2, 2013
Accepted: January 23, 2014
Published: January 23, 2014

   dx.doi.org/10.1021/am404881p | *ACS Appl. Mater. Interfaces* 2014, 6, 2459−2470

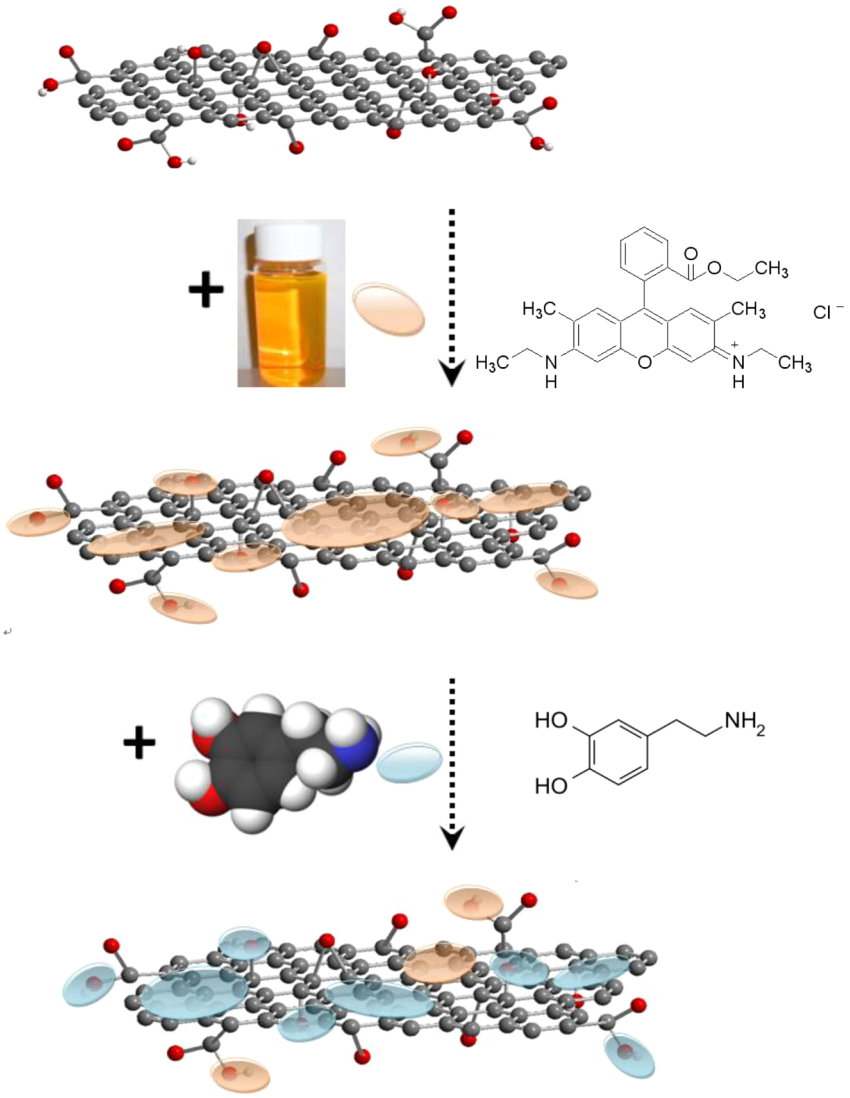

Figure 1. Adsorption and desorption of different molecules on GO due to competitive adsorption.

ions (Pb^{2+}, Cd^{2+}, and Cu^{2+}),[26−28] fluoride ions,[29] dyes (methyl orange,[30] methylblue,[31] and rhodamine B[32]), and detection of biological molecules (DNA[33,34]and tetracycline antibiotics[35]) from aqueous solutions. Yang et al. noted[36] that Cu^{2+} adsorption on graphene oxide at pH 5.0 and T = 293 K could be aggregated with the adsorption capacity of 46.6 mg/g. Zhao et al. found that the maximum adsorption capacities of Cd(II) and Co(II) on GO at pH = 6.0 and T = 303 K were about 106.3 and 68.2 mg/g, respectively.[37] Several studies have been reported on the adsorption of organic species compounds on the surface of GO in aqueous solution, such as DNA, methylene blue,[38] methyl violet, Rhodamine B, orange G,[39] and tetracycline antibiotics. It has been reported that DNA adsorption/desorption properties on GO can be used to detect metal ions,[40,41] small molecules,[42] proteins,[43] and virus.[8] Thus, the dispersions of graphene oxide exhibit great potential applications for the bio/chemical detection as well as environmental treatment.

The intrinsic fluorescence of GO in the visible and NIR ranges makes it attractive for colorimetric sensing.[44] Chen et al. reported the multiple noncovalent interactions between GO and dopamine (DA) resulted in effective self-assembly of DA molecules on the surface of GO and significant fluorescence quenching.[45] Few studies have been reported on the competitive adsorption of multiple chemical compounds on the surface of GO sheets.[46,47] As is known, the adsorption action of GO is dependent on many effects, such as its specific surface area, ratio of sp^2/sp^3 sites, amphiphilic characteristics, or solution composition with some direct correlations such as amphiphilicity (related to sp^2/sp^3 coexisting structures) (Figure 1).[48] Further studies are critical for the understanding of selectivity mechanisms in graphene oxide-based absorbers.

Herein, we investigated the competitive adsorption of common fluorescent dye, Rhodamine 6G (R6G), in direct comparison with dopamine (DA), a representative bioanalyte which is an important biomarker for a number of health issues such as stresses.[49] These biomolecules are derivatives of tyrosine and important to monitor due to their ability to evaluate stress levels, cognitive ability, and fatigue. We selected R6G as a well-known surface-active compound with $\pi-\pi$ and weak interactions for bioengineering applications related to colorimetric sensors.[50,51] To get the maximum adsorption capacities, fluorescence measurements were used as the aid to characterize the exact concentration of analytes. This study demonstrated competitive dopamine adsorption which resulted in partial desorption of R6G molecules from the surface of GO

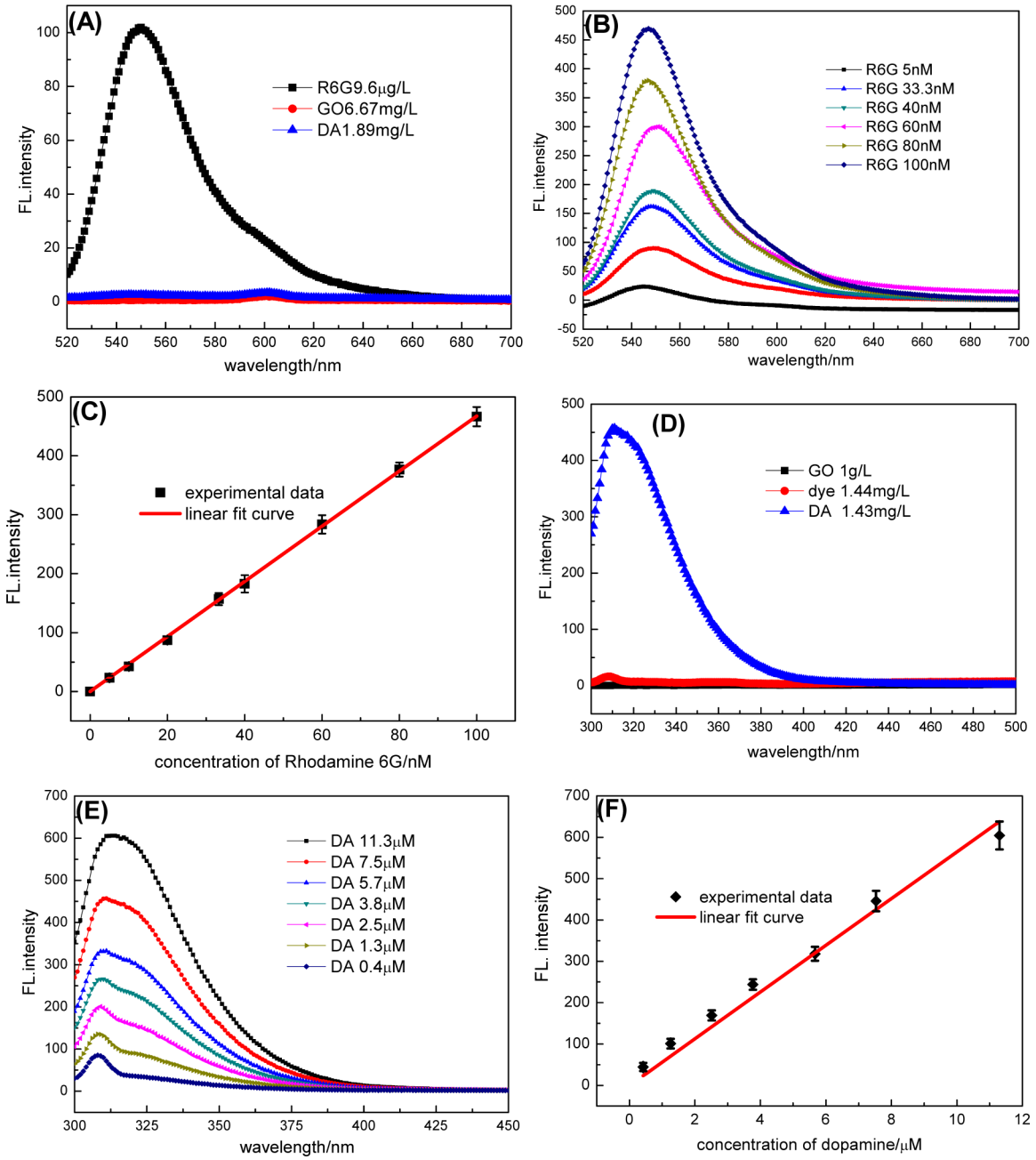

Figure 2. (A) Fluorescence spectra of R6G, GO, and DA excited at 500 nm. (B) Fluorescence spectra of different concentrations of R6G excited at 500 nm. (C) Concentration of R6G versus fluorescence at a peak of 545 nm. (D) Fluorescence spectra of R6G, GO, and DA excited at 280 nm. (E) Fluorescence spectra of different concentrations of DA excited at 280 nm. (F) Concentration of DA versus fluorescence at a peak of 315 nm.

into the solution that can be used for the direct detection of bioanalyte presence in solution (Figure 1).

EXPERIMENTAL SECTION

Chemicals and Materials. R6G was purchased from Sigma Aldrich, and dopamine hydrochloride was purchased from Alfa Aesar. All chemicals were of analytical reagent grade and were used as received. The stock solutions of R6G and DA were prepared by dissolving them in Nanopure water (18.2 MΩ-cm), and the required concentration of working solution was obtained by further diluting the stock solution. GO was synthesized through natural graphite powder by Hummers method as described elsewhere.[52,53]

Instrumentation and Characterization. Fluorescence measurements were performed with a Shimadzu RF-5301PC equipped with a 150 W xenon lamp. The widths of both the excitation slit and emission slit were set at 5.0 mm. ATR-FTIR spectra of the adsorbents were recorded with a FTIR Spectrometer (Vertex, Bruker 70) over the wave range from 4000 to 400 cm^{-1}. Spectral data were measured using a MIRacle single reflection ATR accessory on an FTIR spectrometer. Liquid samples were dropped on the whole surface of diamond crystal and dried at room temperature. All spectral data were collected at 4 cm^{-1} resolution.

Measurement Procedures. In order to measure concentration of R6G and DA in solution, we collected the fluorescence spectra at different concentrations of compounds. The regression coefficients of the calibration curve were 0.998 for R6G and 0.990 for DA, respectively, that facilitates the evaluation of the concentration of free R6G or DA in water solution via measuring fluorescence intensity.

To measure the optical characteristics of the R6G−GO mixture, R6G (200 nM, 1 mL) and GO solution (2, 5, 10, 20, and 50 mg/L, 1 mL) were sequentially added to a 3 mL calibrated test tube. Similarly,

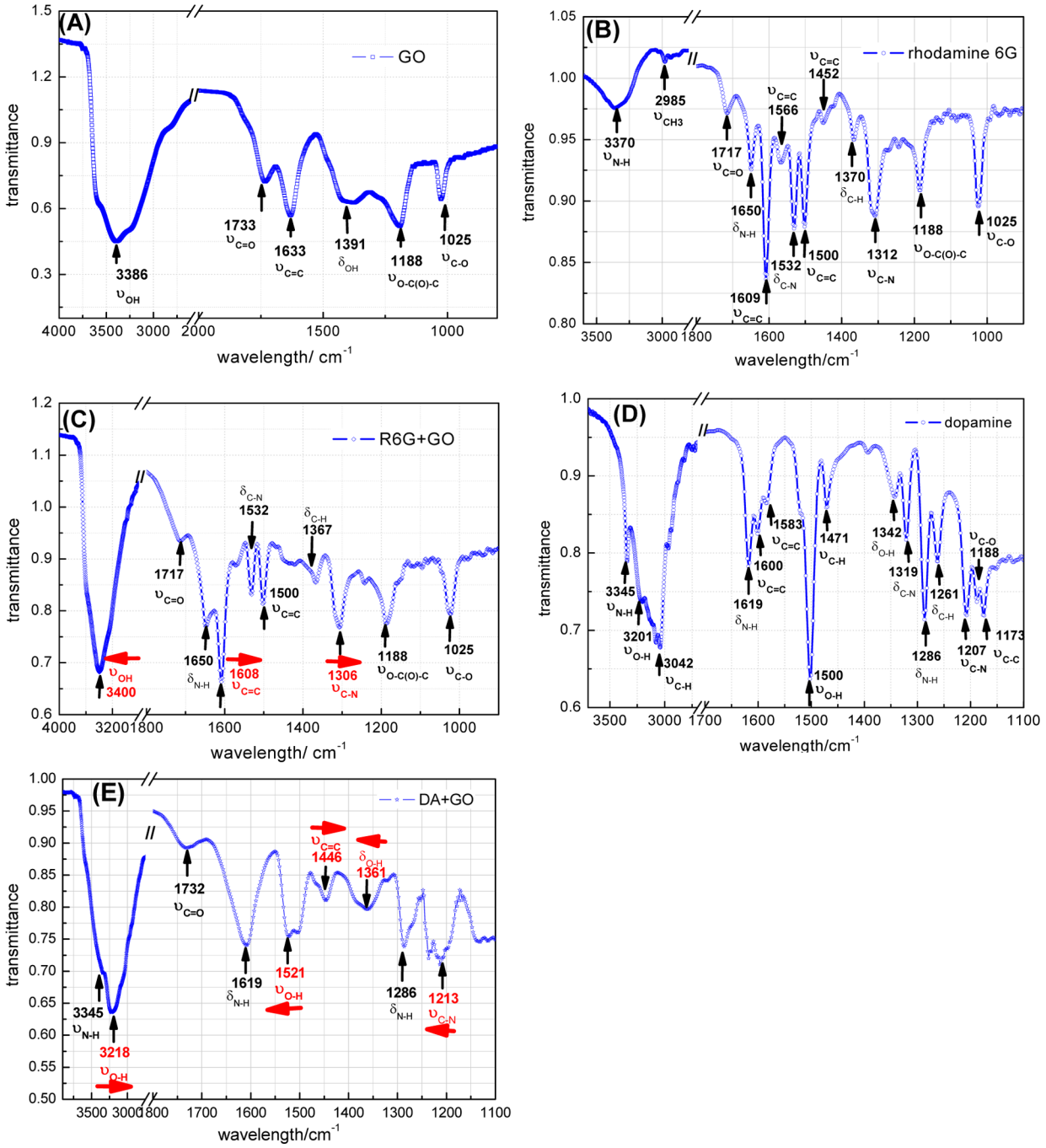

Figure 3. FTIR spectra for (A) GO; (B) R6G; (C) R6G + GO; (D) dopamine; and (E) dopamine + GO solutions.

the optical characteristics of the DA−GO mixture were analyzed by mixing GO solution (1g/L, 1 mL) and dopamine hydrochloride in a 3 mL calibrated test tube. The concentration of diluted DA was 1, 2, 4, 6, 8, and 10 μM, respectively. Finally, to a 3 mL calibrated test tube, R6G solution (180 nM, 1 mL), GO solution (5, 7.5, 10, 12.5, and 15 mg/L, 1 mL), and dopamine hydrochloride (6 μM, 1 mL) were sequentially added. We measure the fluorescence intensity of mixed solution when excitation wavelengths are 280 and 500 nm, respectively.

RESULTS AND DISCUSSION

Adsorption Sites on Graphene Oxide. Figure 2A shows that the characteristic emission peak of R6G is located at 545 nm when excitation wavelength is 500 nm. In contrast, spectra of GO and DA components show a very low emission even at higher concentrations, and thus, these spectral contributions can be ignored for this excitation condition. The intensity of the emission peak has been monitored for different concentrations of R6G and DA, and peak intensities depended upon concentration in a linear fashion (Figure 2B−F).

In order to characterize the possible adsorption sites on GO sheets, FTIR studies have been conducted for different solutions (Figure 3A). Traditional strong peaks were observed on FTIR spectra for GO material: the peak at 1633 cm^{-1} corresponds to the stretching vibration of C═C in the unoxidized graphitic domain, and the oxidized surface regions are evident by the stretching vibration of carboxyl C═O and bending vibration of O−H at the edges of the GO sheets at 1733 and 1391 cm^{-1}, respectively.[54−56] The additional band at

dx.doi.org/10.1021/am404881p | ACS Appl. Mater. Interfaces 2014, 6, 2459−2470

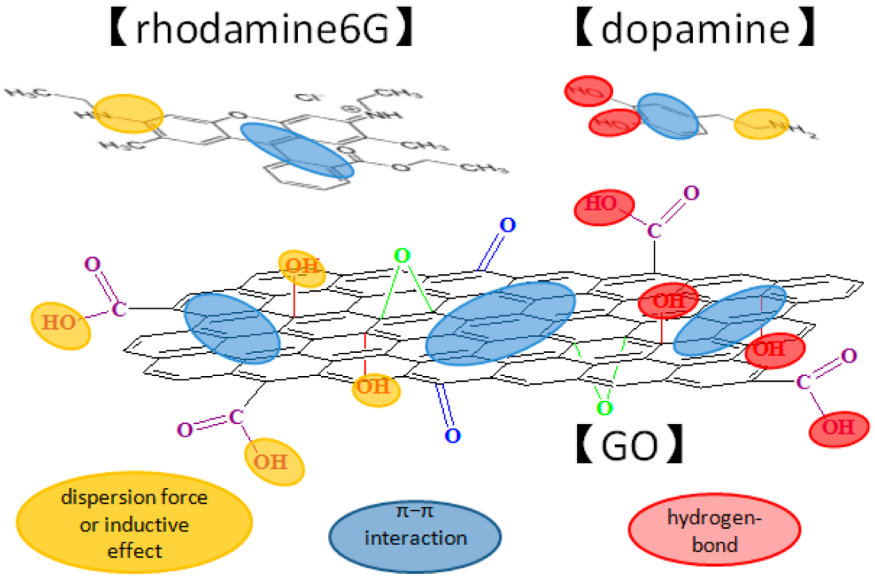

Figure 4. Possible adsorption sites of GO sheets for molecules studied.

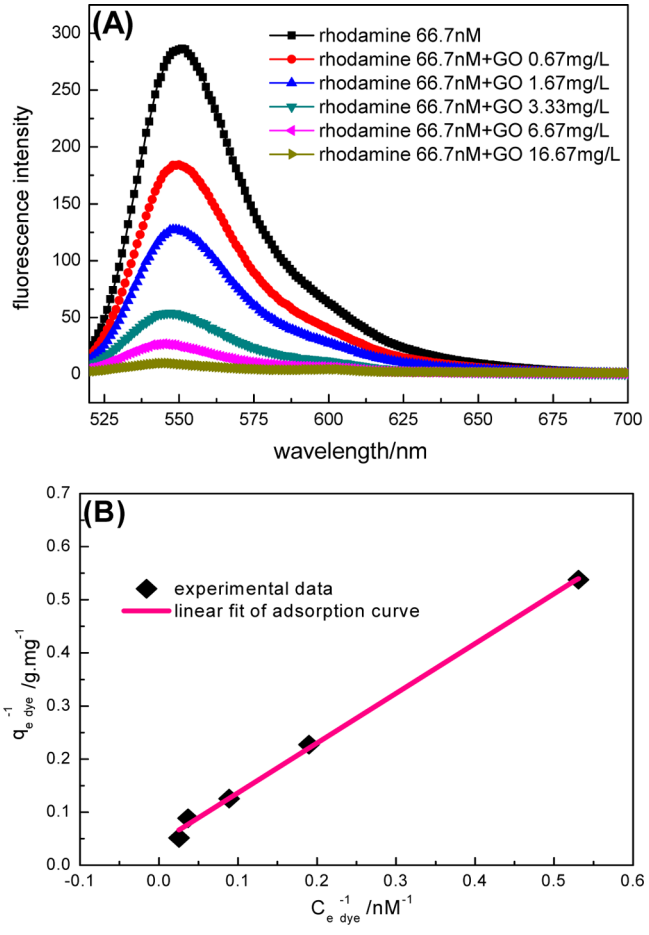

Figure 5. (A) Fluorescence quenching of R6G with increasing concentration of GO component. (B) Langmuir adsorption isotherm of R6G adsorbed on GO material at room temperature.

1025 cm^{-1} corresponds to the stretching vibration of C−O groups; the peak at 1188 cm^{-1} is related to the vibration of epoxy groups (C−C(=O)−O), and the broad band at 3386 cm^{-1} corresponds to the −OH vibration stretching. As we know, the sharp bands of free −OH should be located at 3650−3610 cm^{-1}. With the increasing degree of intermolecular association, the vibrational peaks will broaden and shift to lower frequency. The hydroxyl peak of GO is located at about 3386 cm^{-1} suggesting a certain amount of intramolecular hydrogen bonding.

FTIR spectra of R6G solution show a band at 1716 cm^{-1}, which corresponds to the C=O vibration in ester group, and the bands at 3370 and 1650 cm^{-1} correspond to the N−H stretching vibration and scissor bending vibration of the amine groups (Figure 3B).[57] The bands at 1609, 1566, 1500, and 1452 cm^{-1} correspond to the vibration of aromatic ring skeleton, and the bands at 2985 and 1370 cm^{-1} are C−H stretching vibration and bending vibration of methyl, respectively. Additionally, 1532 and 1312 cm^{-1} peaks are the in-plane bending vibration and stretching vibration of C−N group, respectively. Finally, R6G also showed a band at 1188 and 1025 cm^{-1} similar to that in the GO component.

The FTIR spectra of R6G−GO complex showed a blue shift in the 3386 cm^{-1} peak of GO, representing the hydroxyl on the surface of GO, shifted to 3400 cm^{-1} (Figure 3C). Moreover, the C−N stretching vibration of R6G red-shifted from 1313 to 1306 cm^{-1}. These shifts can be attributed to strong intermolecular interactions including dispersion forces and inductive effects.[58] As known, GO has a negative surface charge in the aqueous environment due to proton dissociation from the hydroxyl groups. On the other hand, R6G is a positively charged dye and thus has a strong affinity for the negatively charged regions of GO sheets. When GO is added into the dye solution, Coulombic interactions facilitate the preferential interactions of oppositely charged species. Inductive effect between protophilic groups and electrophilic groups can also contribute to these shifts.[59] It must be pointed out that the vibrations of hydroxyl group of R6G−GO shifted to higher frequency. At the same time, vibrations for carbonyl group and ester group of R6G do not change indicating no hydrogen bonding between R6G and GO. We suggest that some −OH groups in GO are bound by intramolecular hydrogen bondings. As a result, chemical groups, which have stronger electronegativity in R6G molecules, do not form hydrogen bonding with GO surfaces. Moreover, in a polycyclic aromatic R6G compound, ester and carbonyl groups are influenced by space

dx.doi.org/10.1021/am404881p | ACS Appl. Mater. Interfaces 2014, 6, 2459−2470

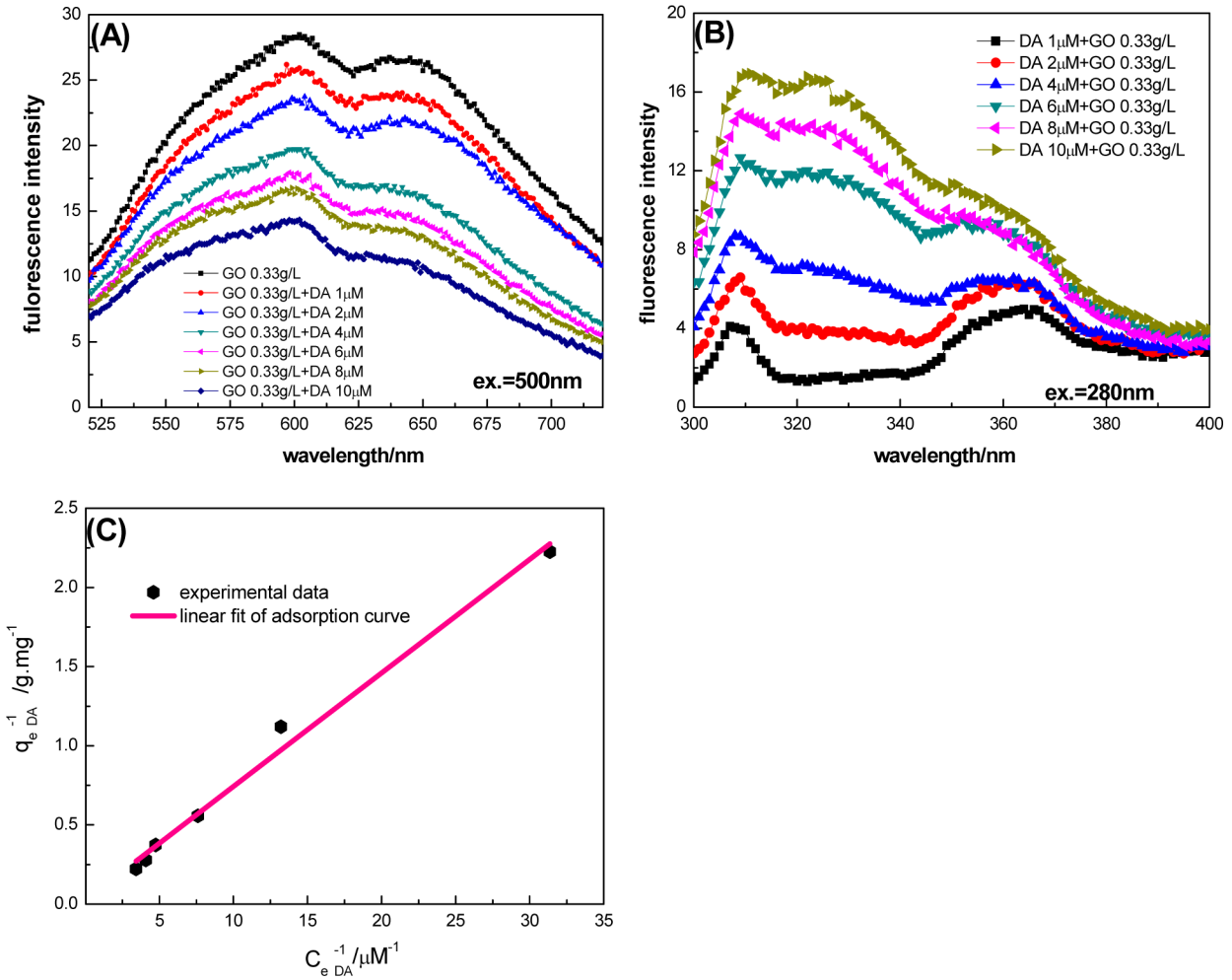

Figure 6. (A) Fluorescence quenching of GO component with increasing concentration of DA excited at 500 nm. (B) Fluorescence quenching of GO with increasing concentration of DA excited at 280 nm. (C) Langmuir adsorption fit of DA to GO.

steric effect and restrictions on forming hydrogen bonding. Consequently, the vibrational peak of −OH groups in R6G−GO complex shifted to higher frequency.

On the other hand, the band at 1633 cm^{-1} (stretching vibration of C═C) shifted to low frequency to 1608 cm^{-1} in R6G solution. This significant shift can be attributed to the $\pi-\pi$ conjugative effect and hydrophobic interactions of selected surface areas with R6G molecules. These regions contain phenyl rings that are also hydrophobic and have a strong tendency to aggregate with the hydrophobic domains of GO.[60] Indeed, GO has been known to have a selective adsorption ability to those aromatic compounds with benzene rings through strong $\pi-\pi$ interactions.[61,62]

On the other hand, FTIR spectra of DA solutions showed characteristic bands at 3345 cm^{-1}, which correspond to the N−H vibration stretching, bands at 1600 and 1583 cm^{-1} for the stretching vibration of C═C of the benzene ring of DA, and bands at 1500 and 1619 cm^{-1} showing the O−H vibration stretching of diols of DA and N−H in plane bending, respectively (Figure 3D). Finally, the bands at 1346 and 1286 cm^{-1} correspond to O−H and N−H bending in plane, and the band at 1207 cm^{-1} corresponds to the C−H bending vibration.[45]

However, the FTIR spectrum of GO−DA mixed solution shows the stretching vibration peak of hydroxyl group red-shifted from 3386 to 3218 cm^{-1} and bending vibration peak shifted from 1342 to 1361 cm^{-1} suggesting a strong hydrogen bonding (Figure 3E).[45] Hydrogen bonding association led to the peak of hydroxyl group broadened and red-shifted. In addition, the spectrum for the GO−DA complex solution shows a band at 1521 cm^{-1}, 21 cm^{-1} higher than that for −OH vibration stretching of diols in DA alone, likely due to the hydrogen-bonding interaction of the diols in DA with GO. Also, the frequency of C−N stretching vibration shifts from 1207 cm^{-1} in DA solution to 1213 cm^{-1} in the GO−DA mixed solution. The band for the stretching vibration of C═C in the unoxidized graphitic domain of the DA−GO complex showed a significantly lower frequency (1446 cm^{-1}) than that in free GO (1500 cm^{-1}) due to strong $\pi-\pi$ interactions. These results suggest strong multiple noncovalent interactions between GO sheets and DA components including multiple hydrogen-bonding and $\pi-\pi$ interactions.[58,59]

From comparison of FTIR results for DA−GO and R6G−GO mixed solutions, it is evident that some characteristic peaks of GO undergo shifts that confirm the formation of the DA−GO and R6G−GO complexes via noncovalent interactions, but no strong chemical interactions (such as covalent bonding) occurred. Moreover, we can suggest that the intermolecular interactions of DA−GO complexes must be stronger than those in the case of R6G−GO because hydrogen bond formation takes place in the DA−GO complex in addition to $\pi-\pi$ interactions. Furthermore, we also found that similar

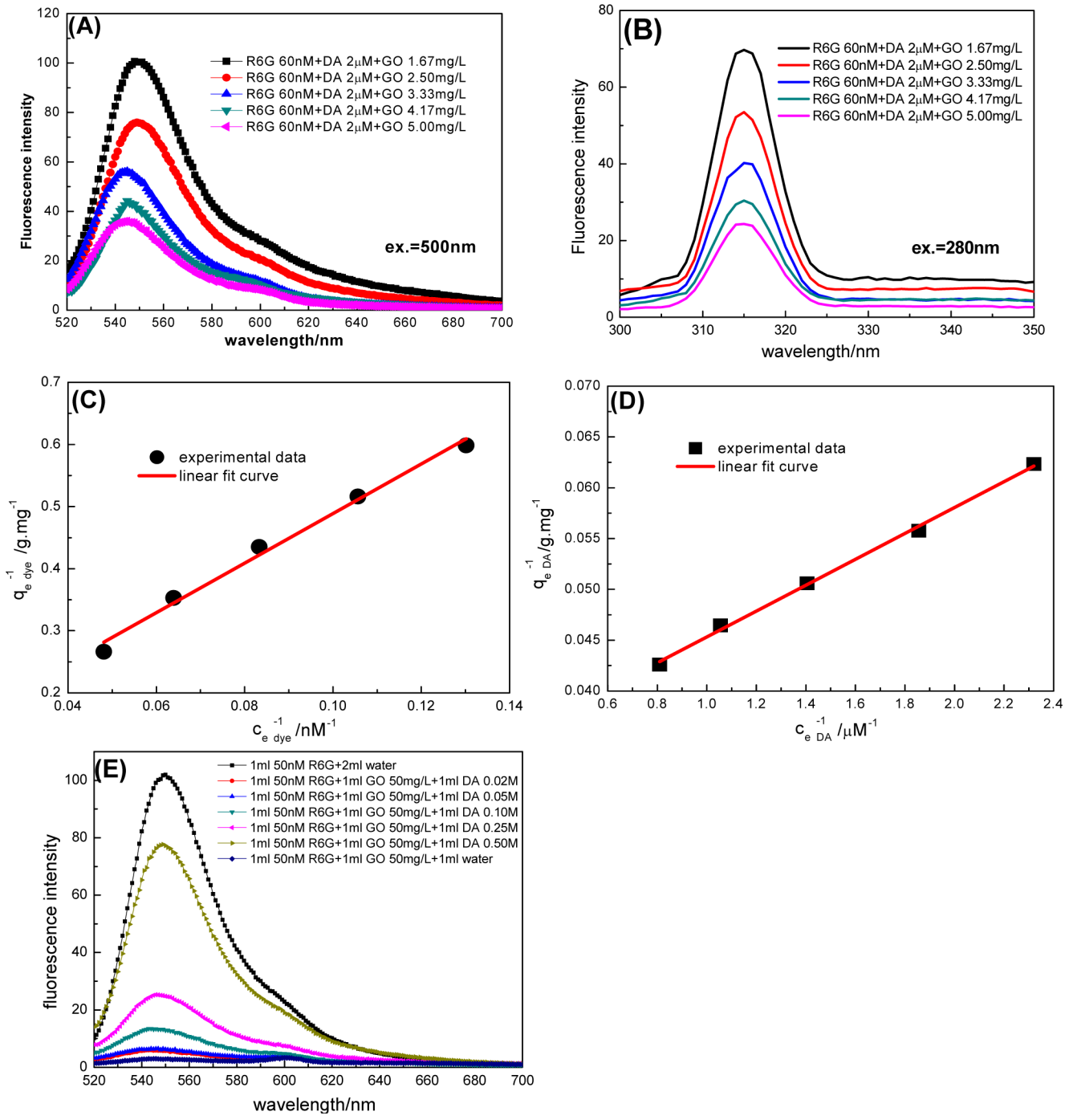

Figure 7. Fluorescence spectra of DA−R6G−GO mixed solutions at 500 nm (A) and 280 nm (B) excitations. (C) Langmuir adsorption isotherms of R6G (D) and DA (C) adsorbed on GO in mixed solutions. (E) Fluorescence recurring when DA was added into the R6G−GO system.

Table 1. Experimental Data of Absorption Parameters in Mixed Solution

[GO], mg/L	C_{e_dye}, nM	C_{e_DA}, μM	q_{e_dye}, mg/g	q_{e_DA}, mg/g
5.00	20.78	1.24	3.76	23.48
7.50	15.64	0.95	2.83	21.53
10.00	12.00	0.71	2.30	19.76
12.50	9.47	0.54	1.94	17.93
15.00	7.68	0.43	1.67	16.05

Table 2. Calculated Data of Absorption Parameters in Mixed Solution

[GO], mg/L	C_{e_dye}, nM	C_{e_DA}, μM	q_{e_dye}, mg/g	q_{e_DA}, mg/g
5.00	26.72	1.13	2.94	29.30
7.50	19.52	0.79	2.58	24.72
10.00	13.17	0.55	2.24	22.20
12.50	9.33	0.40	1.94	19.63
15.00	7.01	0.30	1.69	17.33

interactions exist for the C═C bonds and hydroxyl groups including basal plane and edges of GO sheets. Since the FTIR spectra showed the most significant peak shifts for C═C and O−H groups, we can suggest the corresponding locations of

dx.doi.org/10.1021/am404881p | ACS Appl. Mater. Interfaces 2014, 6, 2459−2470

Table 3. Maximum Adsorption Capacity (x_m) and Free Energy (ΔG^θ) of Adsorption for Common Chemicals, Ions, and Biomolecules

adsorbent	absorbate	x_m, mg/g	ΔG^θ, kJ/mol	refs.
graphene oxide	Rhodamine 6G	23.3	−2.3	this study
graphene oxide	dopamine	40.0	−7.3	this study
graphene oxide	methylene blue	714		35
graphene oxide nanosheets	methyl green	646.9	−2.9	70
graphene	methyl blue	1520	−9.2	71
GO/calcium alginate composites	methylene blue	181.8	−11.6	72
graphene/Fe_3O_4 composites	methylene blue	43.8	−3.9	73
three-dimensional GO	methylene blue	397	−47.7	67
magnetic chitosan graphene	methyl blue	95.1	−0.7	31
three-dimensional GO	methyl violet	467	−68.2	67
graphene oxide	Au(III)	108.3	−0.9	74
graphene oxide	Pt(II)	71.4	−0.2	73
few-layered GO nanosheets	Co(II)	68.2	−20.7	3
few-layered GO nanosheets	Cd(II)	106.3	−2.97	3
magnetite/GO composite	Co(II)	12.9	−19.9	75
chitosan/GO composites	Au(III)	1080	−10.2	76
chitosan/GO composites	Pd(II)	220	−8.8	76
GO nanosheets	Eu(III)	175.4	−24.9	28
sulfur/reduced GO nanohybrid	mercury ions		−21.9	77
graphene	fluoride	17.7	−0.1	78
RGO/magnetite composites	ciprofloxacin	18.2	−20.3	79
RGO/magnetite composites	norfloxacin	22.2	−20.5	79
graphene	Bisphenol A	182	−10.3	60
graphene	P-toluenesul acid	1430		71
graphene	1-naphthalenesulfonic acid	1460		71

possible adsorption sites (Figure 4). On the other hand, R6G or DA molecules might adsorb on the hydrophobic regions of GO sheets due to $\pi-\pi$ interactions and dopamine further interacts with hydroxyl groups of GO sheets due to hydrogen bonding.

Adsorption Kinetics. To further understand the adsorption and readsorption behavior, we studied the adsorption isotherms by monitoring R6G fluorescent peak intensity and using conventional adsorption approaches as briefly summarized below. As is known, the adsorption capacity, q_e, can be calculated from adsorption isotherms using the following equation:[63]

$$q_e = \frac{V(C_o - C_e)}{m} \quad (1)$$

where C_o and C_e are initial and equilibrium concentrations of compound of interest (in mg/L), respectively, m is the mass of adsorbent (in g), and V is the volume of the solution (in L).

From this data, the Langmuir isotherm can be obtained assuming a surface with homogeneous binding sites, equivalent sorption energies, and no interaction between adsorbed species:[63]

$$\frac{1}{q_e} = \frac{b}{x_m C_e} + \frac{1}{x_m} \quad (2)$$

where q_e is the equilibrium adsorption amount of compound (in mg/g), C_e is the equilibrium concentration in the aqueous solution (in mg/mL), x_m is the maximum adsorption amount per mg of adsorbent (in mg/g), and b is the Langmuir adsorption equilibrium constant (in mol/L).

The constants in eq 2 have a strong theoretical basis:[64] x_m correlates with the surface concentration and monolayer coverage and denotes the maximum adsorbed amount that can be obtained as the equilibrium concentration of the solute is increased. The other Langmuir equation constant, b, represents the energy associated with adsorption and increases as the strength of the adsorption bond increases. The constant values in the equation can be determined from the analysis of the linear plot of $1/q_e$ versus $1/C_e$. If b is known, the free energy of adsorption, ΔG^θ, can be calculated using the equation:[62]

$$\log b = \frac{\Delta G^\theta}{2.3RT} + 1.74 \quad (3)$$

where, ΔG^θ is the free energy of adsorption (in kJ/mol), R is gas constant, and T is temperature (in K).

For competitive adsorption of two molecules A and B, which (i) are both adsorbed molecularly and (ii) compete for the same adsorption sites, the Langmuir model can be used to derive a modified adsorption isotherm:[64]

$$q_1 = \frac{x_{m,1} \times b_1 \times C_{e,1}}{1 + b_1 \times C_{e,1} + b_2 \times C_{e,2}} \quad (4)$$

$$q_2 = \frac{x_{m,2} \times b_2 \times C_{e,2}}{1 + b_1 \times C_{e,1} + b_2 \times C_{e,2}} \quad (5)$$

where q_1 and q_2 are the amount of solute (1 or 2) adsorbed per unit weight of adsorbent at equilibrium concentrations and $x_{m,1}$ and $x_{m,2}$ are maximum values of x_1 and x_2, respectively, that are obtained from single-solute isotherm analysis, which correspond to monolayer coverage of the adsorbent. Here, b_1 and b_2 are constants that are a function of the energy of adsorption and are obtained from single-solute isotherm analysis.[65]

Single Component R6G Adsorption. The adsorption of R6G on GO at different GO concentrations was analyzed by monitoring the change in its fluorescence intensity at a fixed R6G concentration (Figure 5A). First, we observed that, upon addition of GO to the R6G solution, the fluorescence intensity reduced significantly due the adsorption of R6G molecules on the GO surface and the quenching of R6G fluorescence.[66]

Analyzing the fluorescence intensity of the mixed R6G−GO solution with the change in GO concentration, we calculated the concentration of free R6G dye in solution and considered it as the equilibrium concentration of R6G after adsorption. The plot of $1/q_e$ vs $1/C_e$ (Langmuir isotherm coordinates) yielded a straight line that indicates the Langmuir behavior. From the

slope and intercept of linear approximation, the values of $x_{m\text{-}R6G}$ and b_{R6G} were estimated to be 23.3 mg/g and 21.7 nM, respectively (Figure 5B). In addition, from this data, we estimated the free energy of adsorption of R6G−GO complex ($\Delta G^{\theta}_{R6G-GO}$) to be −2.3 kJ/mol. SinceΔG^{θ} is negative and low, we can conclude that the R6G adsorption process is spontaneous and the adsorption is controlled by weak molecular interactions as was suggested from the FTIR data analysis.[67]

Individual Dopamine Absorption. In order to monitor the adsorption of dopamine, the fluorescence spectra of DA−GO complex were measured at 500 nm excitation wavelength because GO has weak fluorescence emission. The results show that fluorescence intensity declines with the increase in dopamine concentration due to quenching of GO component (Figure 6A).

To get the adsorption isotherms of mixed DA−GO solution, the exact equilibrium concentrations of DA in solution must be determined. Thus, we measured the fluorescence spectrum of the same DA−GO complex under the excitation wavelength of 280 nm (Figure 6B). The fluorescence peak at 315 nm is identified at a concentration of free dopamine determined from Figure 2B. The corresponding Langmuir adsorption isotherm obtained from this data can be described by a regular linear regression (R^2 = 0.99) (Figure 6C). Thus, saturated adsorption capacity of DA ($x_{m\text{-}DA}$) of 40.0 mg/g and Langmuir adsorption equilibrium constant b_{DA} of 2.88 μM can be determined. Finally, the free energy of adsorption $\Delta G^{\theta}_{DA-GO}$ = −7.30 kJ/mol was obtained for the DA−GO complex. The absolute value of $\Delta G^{\theta}_{DA-GO}$ is significantly larger than $\Delta G^{\theta}_{R6G-GO}$ determined above for R6G; $\Delta G^{\theta}_{DA-GO}$ suggests that DA molecules have much stronger affinity to the GO surface in comparison with R6G dye.

Adsorption from Mixed Solutions. To understand the competitive adsorption action of two different compounds on the surface of GO sheets, the concentration of GO component varied in the mixed solution while keeping the concentration of R6G and DA components constant. Figure 7 shows the fluorescence spectra of mixed DA−R6G−GO solutions at 280 and 500 nm excitation wavelengths. Since there are no strong interactions between DA and R6G components,[68] the equilibrium concentrations can be determined by converting the fluorescence intensities to concentration using a predetermined linear calibration graph. The same method was used to estimate the equilibrium concentration of components in binary solutions.

From this data, we calculated the mass per gram of adsorbents and equilibrium concentrations of the two components adsorbed by GO using eq 1 (Table 1).The results of these evaluations show that the equilibrium concentrations of R6G and DA components gradually decline with increasing concentration of GO component. The adsorbed mass per gram shows the same downtrend. We further analyzed the data in Table 1 and obtained the adsorption coefficients by plotting absorbance (mass per gram) versus the equilibrium concentration of each component. The results obtained correspond to the linear fit expected from a Langmuir adsorption (Figure 7C,D). The slope of the corresponding linear regression gave the value of the absorptive coefficients for each component (Table 1). The saturation adsorption capacity of R6G component declined from 23.3 to 11.2 mg/g, and at the same time, the value of adsorbed DA component decreased from 40.0 to 31.3 mg/g.

The experimental data further validated that R6G and DA molecules compete for similar adsorption sites at the GO surface. It can be ascertained that the adsorption of DA molecules can lead to desorption of R6G molecules from the GO surface owing to its weak physical adsorption on the surface with low free energy adsorption. At the same time, we found the maximum adsorption capacity of R6G component descends more rapidly than that for DA molecules. This result clearly indicates that dopamine predominates in competitive adsorption from mixed solution due to a stronger affinity to GO surface. To further analyze whether the presence of dopamine molecules affected the adsorption of R6G molecules, the adsorption capacities of each component in mixture solutions were computed using eqs 1, 4, and 5). Here, we substitute the adsorption parameters obtained from single-solute isotherm analysis to eqs 4 and 5 to obtain the values of q_1, q_2, C_{e1}, and C_{e2} and confirm the applicability of the model to mixed solutions (Table 2).

From comparison of saturation adsorption capacities and equilibrium adsorption amounts of R6G and DA components in the mixed solution, we can conclude that R6G adsorption saturates faster. Thus, DA molecules possess higher affinity toward active adsorption sites and higher priority in the monolayer saturation. Adding DA component to the mixed R6G−GO solution caused competitive adsorption of this component on active sites on the GO surface, which might lead to the reduction of R6G coverage and partial release of R6G into the solution. Indeed, we observed that adding DA component to mixed R6G−GO solution resulted in the R6G fluorescence increase as a result of forced desorption of R6G from the GO surface into solution and the reduction of fluorescent quenching (Figure 7E).

Finally, to compare the adsorption abilities of different compounds, we analyzed the experimental data for free energy of adsorption of various metal ions, popular dyes, and biomolecules to the surface of GO materials in Table 3. As can be seen from direct comparison of different compounds in Table 3, GO can easily bind some important compounds at room temperature with very high binding energy. Considering that R6G is weakly bound to GO sheets (only −2.3 kJ/mol), a number of other important compounds with stronger interactions can displace this fluorescent dye from the GO surface to a free solution. The corresponding increase in fluorescent intensity might serve for colorimetric detection of the presence of various strongly binding components in solution.

CONCLUSIONS

In conclusion, we found that both R6G and dopamine molecules are readily absorbed on the surface of GO sheets with the adsorption behavior described by the traditional Langmuir isotherms. Both components are anchored to similar oxidized surface sites via complex weak intermolecular interactions with the affinity to the GO surface much higher for dopamine molecules (adsorption energy of −7.5 vs −2.3 kJ/mol for R6G compound). This difference results in a competitive adsorption phenomenon leading to the displacement of quenched R6G molecules adsorbed on the GO surface with the strongly adsorbing DA component in the mixed solution when DA component is added to R6G−GO complexes. Such a process results in dramatically increased emission that can be readily monitored with characteristic fluorescence of free R6G components.

Competitive adsorption action on the surface of highly dispersible GO component can be considered as a straightforward routine for the detection of trace levels of dopamine, an important biomarker,[69] in complex biofluids. This phenomenon might be considered as a base for prospective sensing applications in biotechnology, biosensing, and environmental science. For instance, the presence of dopamine molecules discussed in this study in blood indicates a rapid increase in the basal metabolic rate which can have a dramatic effect on the subsequent production of other biomolecules. The concentration of dopamine in the blood can be an indicator of an individual's current state of stress and alertness and thus is needed to be readily and quickly detected by facile and reliable colorimetric sensors.

AUTHOR INFORMATION

Corresponding Author

*E-mail: vladimir@mse.gatech.edu.

Author Contributions

‡H.R. and D.D.K. contributed equally.

Notes

The authors declare no competing financial interest.

ACKNOWLEDGMENTS

This research was supported by National Natural Science Foundation of China, State Scholarship Fund of China Scholarship Council, opening project of State Key Laboratory of Explosion Science and Technology, the Semiconductor Research Corporation (GRC Grant 2008OJ1864.1281), Air Force Office of Scientific Research (AFOSR Grant FA9550-11-1-0233), and National Science Foundation (Grant DMR-1209332).

REFERENCES

(1) Zhu, Y. W.; Murali, S.; Cai, W. W.; Li, X. S.; Suk, J. W.; Potts, J. R.; Ruoff, R. S. Graphene and graphene oxide: Synthesis, properties and applications. *Adv. Mater.* **2010**, *22*, 3906−3924.

(2) Huang, X.; Yin, Z. Y.; Wu, S. X.; Qi, X. Y.; He, Q. Y.; Zhang, Q. C.; Yan, Q. Y.; Boey, F.; Zhang, H. Graphene-based materials: Synthesis, characterization, properties, and applications. *Small* **2011**, *7*, 1876−1902.

(3) Zhao, G. X.; Li, J. X.; Ren, X. M.; Chen, C. L.; Wang, X. K. Few layered graphene oxide nanosheets as superior sorbents for heavy metal ion pollution management. *Environ. Sci. Technol.* **2011**, *45*, 10454−10462.

(4) James, A. M.; Harry, B. M.; Michael, D. M.; Walter, J. W.; John, C. C. Surface chemistry of active carbon: Specific adsorption of phenols. *J. Colloid Interface Sci.* **1969**, *31*, 116−130.

(5) Yu, J. S.; Kang, S.; Yoon, S. B.; Chai, G. Fabrication of ordered uniform porous carbon networks and their application to a catalyst supporter. *J. Am. Chem. Soc.* **2002**, *124*, 9382−9383.

(6) Peigney, A.; Laurent, C. H.; Flahaut, E.; Bacsa, R. R.; Rousset, A. Specific surface area of carbon nanotubes and bundles of carbon nanotubes. *Carbon* **2001**, *39*, 507−514.

(7) Kim, J. Y.; Cote, L. J.; Kim, F.; Yuan, W.; Shull, K. R.; Huang, J. X. Graphene oxide sheets at interfaces. *J. Am. Chem. Soc.* **2010**, *132*, 8180−8186.

(8) Jung, J. H.; Cheon, D. S.; Liu, F.; Lee, K. B.; Seo, T. S. A graphene oxide based immuno-biosensor for pathogen detection. *Angew. Chem., Int. Ed.* **2010**, *49*, 5708−5711.

(9) Song, Y. J.; Qu, K. G.; Zhao, C.; Ren, J. S.; Qu, X. G. Graphene oxide: Intrinsic peroxidase catalytic activity and its application to glucose detection. *Adv. Mater.* **2010**, *22*, 2206−2210.

(10) Wen, Y. Q.; Xing, F. F.; He, S. J.; Song, S. P.; Wang, L. H.; Fan, C. H. A graphene-based fluorescent nanoprobe for silver(I) ions detection by using graphene oxide and a silver-specific oligonucleotide. *Chem. Commun.* **2010**, *46*, 2596−2598.

(11) Wu, D.; Zhang, F.; Liang, H.; Feng, X. Nanocomposites and macroscopic materials: Assembly of chemically modified graphene sheets. *Chem. Soc. Rev.* **2012**, *41*, 6160−6177.

(12) Kuilla, T.; Bhadra, S.; Yao, D.; Kim, N. H.; Bose, S.; Lee, J. H. Recent advances in graphene based polymer composites. *Prog. Polym. Sci.* **2010**, *35*, 1350−1375.

(13) Yang, M.; Hou, Y.; Kotov, N. A. Graphene-based multilayers: Critical evaluation of materials assembly techniques. *Nano Today* **2012**, *7*, 430−447.

(14) Young, R. J.; Kinloch, I. A.; Gong, L.; Novoselov, K. S. The mechanics of graphene nanocomposites: A review. *Compos. Sci. Technol.* **2012**, *72*, 1459−1476.

(15) Hu, K.; Kulkarni, D. D.; Choi, I.; Tsukruk,V. V. *Prog. Polym. Sci.*, in press.

(16) Xu, B.; Yue, S. F.; Sui, Z. Y.; Zhang, X. T.; Hou, S. S.; Cao, G. P.; Yang, Y. S. What is the choice for supercapacitors: Graphene or grapheme oxide? *Energy Environ. Sci.* **2011**, *4*, 2826−2830.

(17) Stankovich, S.; Dikin, D. A.; Piner, R. D.; Kohlhaas, K. A. Synthesis of graphene-based nanosheets via chemical reduction of exfoliated graphite oxide. *Carbon* **2007**, *45*, 1558−1565.

(18) Park, S. J.; An, J.; Potts, J. R.; Velamakanni, A.; Murali, S.; Ruoff, R. S. Hydrazine-reduction of graphite- and graphene oxide. *Carbon* **2011**, *49*, 3019−3023.

(19) Huang, X.; Yin, Z.; Wu, S.; Qi, X.; He, Q.; Zhang, Q.; Yan, Q.; Boey, F.; Zhang, H. Graphene-based materials: Synthesis, characterization, properties, and applications. *Small* **2011**, *7*, 1876−1902.

(20) Compton, O. C.; Nguyen, S. T. Graphene oxide, highly reduced graphene oxide, and graphene: Versatile building blocks for carbon-based materials. *Small* **2010**, *6*, 711−723.

(21) Dreyer, D. R.; Park, S. J.; Bielawski, C. W.; Ruo, R. S. The chemistry of graphene oxide. *Chem. Soc. Rev.* **2010**, *39*, 228−240.

(22) Hu, K.; Gupta, M. K.; Kulkarni, D. D.; Tsukruk, V. V. Ultra-robust graphene oxide-silk fibroin nanocomposite membranes. *Adv. Mater.* **2013**, *25*, 2301−2307.

(23) Erickson, K.; Erni, R.; Lee, Z. H.; Alem, N.; Gannett, W.; Zettl, A. Determination of the local chemical structure of graphene oxide and reduced graphene oxide. *Adv. Mater.* **2010**, *22*, 4467−4472.

(24) Bagri, A.; Mattevi, C.; Acik, M.; Chabal, Y. J.; Chhowalla, M.; Shenoy, V. B. Structural evolution during the reduction of chemically derived graphene oxide. *Nat. Chem.* **2010**, *2*, 581−587.

(25) Kim, F.; Cote, L. J.; Huang, J. X. Graphene oxide: Surface activity and two-dimensional assembly. *Adv. Mater.* **2010**, *22*, 1954−1958.

(26) Madadrang, C. J.; Kim, H. Y.; Gao, G.; Wang, N. Adsorption behavior of EDTA-graphene oxide for Pb (II) removal. *ACS Appl. Mater. Interfaces* **2012**, *4*, 1186−1193.

(27) Mi, X.; Huang, G. B.; Xie, W. S.; Wang, W.; Liu, Y.; Gao, J. P. Preparation of graphene oxide aerogel and its adsorption for Cu^{2+} ions. *Carbon* **2012**, *50*, 4856−4864.

(28) Sun, Y. B; Wang, Q.; Chen, C.; Tan, X.; Wang, X. K. Interaction between Eu(III) and graphene oxide nanosheets investigated by batch and extended X-ray absorption fine structure spectroscopy and by modeling techniques. *Environ. Sci. Technol.* **2012**, *46*, 6020−6027.

(29) Huang, P. J.; Liu, J. W. Molecular beacon lighting up on graphene oxide. *Anal. Chem.* **2012**, *84*, 4192−4198.

(30) Geng, Z. G.; Lin, Y.; Yu, X. X.; Shen, Q. H.; Ma, L.; Li, Z. Y.; Pan, N.; Wang, X. P. Highly efficient dye adsorption and removal: A functional hybrid of reduced graphene oxide−Fe_3O_4 nanoparticles as an easily regenerative adsorbent. *J. Mater. Chem.* **2012**, *22*, 3527−3535.

(31) Fan, L.; Luo, C. N.; Li, X. J.; Lu, F. G.; Qiu, H. M.; Sun, M. Fabrication of novel magnetic chitosan grafted with graphene oxide to enhance adsorption properties for methyl blue. *J. Hazard. Mater.* **2012**, *215−216*, 272−279.

(32) Ai, L. H.; Jiang, J. Removal of methylene blue from aqueous solution with self-assembled cylindrical graphene-carbon nanotube hybrid. *Chem. Eng. J.* **2012**, *192*, 156−163.

(33) He, S. J.; Song, B.; Li, D.; Zhu, C. F.; Qi, W. P.; Wen, Y. Q.; Wang, L. H.; Song, S. P.; Fang, H. P.; Fan, C. H. A graphene nanoprobe for rapid, sensitive, and multicolor fluorescent DNA analysis. *Adv. Funct. Mater.* **2010**, *20*, 453−459.
(34) Li, F.; Huang, Y.; Yang, Q.; Zhong, Z. T.; Li, D.; Wang, L. H.; Song, S. P.; Fan, C. H. A graphene-enhanced molecular beacon for homogeneous DNA detection. *Nanoscale* **2010**, *2*, 1021−1026.
(35) Gao, Y.; Li, Y.; Zhang, L.; Huang, H.; Hua, J. J.; Shan, S. M.; Su, X. G. Adsorption and removal of tetracycline antibiotics from aqueous solution by graphene oxide. *J. Colloid Interface Sci.* **2012**, *368*, 540−546.
(36) Yang, S. T.; Chang, Y. L.; Wang, H. F.; Liu, G. B.; Chen, S.; Wang, Y. W.; Liu, Y. F.; Cao, A. N. Folding/aggregation of graphene oxide and its application in Cu^{2+} removal. *J. Colloid Interface Sci.* **2010**, *351*, 122−127.
(37) Zhao, G. X.; Ren, X. M.; Gao, X.; Tan, X. L.; Li, J. X.; Chen, C. L.; Huang, Y. Y.; Wang, X. K. Removal of Pb(II) ions from aqueous solutions on few-layered graphene oxide nanosheets. *Dalton Trans.* **2011**, *40*, 10945−10952.
(38) Zhang, W. J.; Zhou, C. J.; Zhou, W. C.; Lei, A. H.; Zhang, Q. L.; Wan, Q.; Zou, B. S. Fast and considerable adsorption of methylene blue dye onto graphene oxide. *Bull. Environ. Contam. Toxicol.* **2011**, *87*, 86−90.
(39) Ramesha, G. K.; Kumara, A. V.; Muralidhara, H. B.; Sampath, S. Graphene and graphene oxide as effective adsorbents toward anionic and cationic dyes. *J. Colloid Interface Sci.* **2011**, *361*, 270−277.
(40) Wu, M.; Kempaiah, R.; Huang, P. J.; Maheshwari, V.; Liu, J. W. Adsorption and desorption of DNA on graphene oxide studied by fluorescently labeled oligonucleotides. *Langmuir* **2011**, *27*, 2731−2738.
(41) Liu, J. W. Adsorption of DNA onto gold nanoparticles and graphene oxide: Surface science and applications. *Phys. Chem. Chem. Phys.* **2012**, *14*, 10485−10496.
(42) Hong, B. J.; An, Z. H.; Compton, O. C.; Nguyen, S. T. Tunable biomolecular interaction and fluorescence quenching ability of graphene oxide: Application to "turn-on" DNA sensing in biological media. *Small* **2012**, *8*, 2469−2476.
(43) Mao, S.; Lu, G. H.; Yu, K. H.; Bo, Z.; Chen, J. H. Specific protein detection using thermally reduced graphene oxide sheet decorated with gold nanoparticle-antibody conjugates. *Adv. Mater.* **2010**, *22*, 3521−3526.
(44) Loh, K. P.; Bao, Q. L.; Eda, G.; Chhowalla, M. Graphene oxide as a chemically tunable platform for optical applications. *Nat. Chem.* **2010**, *2*, 1015−1024.
(45) Chen, J. L.; Yan, X. P.; Meng, K.; Wang, S. F. Graphene oxide based photoinduced charge transfer label-free near-infrared fluorescent biosensor for dopamine. *Anal. Chem.* **2011**, *83*, 8787−8793.
(46) Wang, Y.; Li, Z. H.; Wang, J.; Li, J. H.; Lin, Y. H. Graphene and graphene oxide: Biofunctionalization and applications in biotechnology. *Trends Biotechnol.* **2011**, *29*, 205−212.
(47) Lu, C. H.; Yang, H. H.; Zhu, C. L.; Chen, X.; Chen, G. N. A graphene platform for sensing biomolecules. *Angew. Chem.* **2009**, *121*, 4879−4881.
(48) Kim, J. Y.; Cote, L. J.; Kim, F.; Yuan, W.; Shull, K. R.; Huang, J. X. Graphene oxide sheets at interfaces. *J. Am. Chem. Soc.* **2010**, *132*, 8180−8186.
(49) Campbell, N. A.; Reece, J. B.; Mitchell, L. G. *Biology*, 5th ed; Benjamin/Cummings Publications: New York, 1999.
(50) Lunn, G.; Sansone, B. E. *Destruction of Hazardous Chemicals in the Laboratory*; John Wiley & Sons Publication: New York, 2012.
(51) Lversen, L. L. *Dopamine Handbook*; Oxford University Press: Oxford, 2010.
(52) Hummers, W. S., Jr.; Offeman, R. E. Preparation of graphitic oxide. *J. Am. Chem. Soc.* **1958**, *80*, 1339.
(53) Kulkarni, D. D.; Choi, I.; Singamaneni, S.; Tsukruk, V. V. Graphene oxide polyelectrolyte membranes. *ACS Nano* **2010**, *8*, 4667−4676.
(54) Paredes, J. I.; Villar-Rodil, S.; Martínez-Alonso, A.; Tascón, J. M. D. Graphene oxide dispersions in organic solvents. *Langmuir* **2008**, *24*, 10560−10564.
(55) Marcano, D. C.; Kosynkin, D. V.; Berlin, J. M.; Sinitskii, A.; Sun, Z. Z.; Slesarev, A.; et al. Improved synthesis of graphene oxide. *ACS Nano* **2010**, *4*, 4806−4814.
(56) Wang, G. X.; Wang, B.; Park, J.; Yang, J.; Shen, X. P.; Yao, J. Synthesis of enhanced hydrophilic and hydrophobic graphene oxide nanosheets by a solvothermal method. *Carbon* **2009**, *47*, 68−72.
(57) Majoube, M.; Henry, M. Fourier transform Raman and infrared and surface-enhanced Raman spectra for rhodamine 6G. *Spectrochim. Acta, Part A* **1991**, *47*, 1459−1466.
(58) Griffiths, P. R.; De Haseth, J. A. *Fourier Transform Infrared Spectrometry*; John Wiley & Sons Press: New York, 2007.
(59) Maitland, G. C. *Intermolecular forces: their origin and determination*; Clarendon Press: Oxford, 1981.
(60) Xu, J.; Wang, L.; Zhu, Y. Decontamination of Bisphenol A from aqueous solution by graphene adsorption. *Langmuir* **2012**, *28*, 8418−8425.
(61) Liu, Z.; Robinson, J. T.; Sun, X.; Dai, H. PEGylated nanographene oxide for delivery of water-insoluble cancer drugs. *J. Am. Chem. Soc.* **2008**, *130*, 10876−10877.
(62) Zhang, L. M.; Xia, J. G.; Zhao, Q. H.; Liu, L. W.; Zhang, Z. J. Functional graphene oxide as a nanocarrier for controlled loading and targeted delivery of mixed anticancer drugs. *Small* **2010**, *6*, 537−544.
(63) Rodrigues, A. E.; LeVan, D.; Tondeur, D. *Adsorption: Science and Technology*, 3rd ed; Springer Press: Germany, 1989.
(64) Kondo, S.; Ishikanwa, T.; Abe, I. *Adsorption Science*, 2nd ed; Chemical industry press: Beijing, 2005.
(65) Selim, H. M. *Competitive Sorption and Transport of Heavy Metals in Soils and Geological Media*; CRC Press: Boca Raton, 2012.
(66) Morales-Narváez, E.; Merkoçi, A. Graphene oxide as an optical biosensing platform. *Adv. Mater.* **2012**, *24*, 3298−3308.
(67) Liu, F.; Chung, S. Y.; Oh, G.; Seo, T. S. Three-dimensional graphene oxide nano structure for fast and efficient water-soluble dye removal. *ACS Appl. Mater. Interfaces* **2012**, *4*, 922−927.
(68) Liu, Q. Z.; Yu, B.; Ye, W. C.; Zhou, F. Highly selective uptake and release of charged molecules by pH-responsive polydopamine microcapsules. *Macromol. Biosci.* **2011**, *11*, 1227−1234.
(69) Sokoloff, P.; Giros, B.; Martres, M. P.; Bouthenet, M. L.; Schwartz, J. C. Molecular cloning and characterization of a novel dopamine receptor (D_3) as a target for neuroleptics. *Nature* **1990**, *347*, 146−151.
(70) Ponchami, S.; Manash, R. D. Removal of a cationic dye from aqueous solution using graphene oxide nanosheets: Investigation of adsorption parameters. *J. Chem. Eng. Data* **2013**, *58*, 151−158.
(71) Wu, T.; Cai, X.; Tan, S. Z.; Li, H. Y.; Liu, J. S.; Yang, W. D. Adsorption characteristics of acrylonitrile, p-toluenesulfonic acid, 1-naphthalenesulfonic acid and methyl blue on graphene in aqueous solutions. *Chem. Eng. J.* **2011**, *173*, 144−149.
(72) Li, Y. H.; Du, Q. J.; Liu, T. H.; Sun, J. K.; Wang, Y. H.; Wu, S. L.; Wang, Z. H.; Xia, Y. Z. Methylene blue adsorption on graphene oxide/calcium alginate composites. *Carbohydr. Polym.* **2013**, *95*, 501−507.
(73) Ai, L. H.; Zhang, C. Y.; Chen, Z. L. Removal of methylene blue from aqueous solution by a solvothermal-synthesized graphene/magnetite composite. *J. Hazard. Mater.* **2011**, *192*, 1515−1524.
(74) Liu, L.; Liu, S. X.; Zhang, Q. P.; Li, C.; Bao, C. L.; Liu, X. T.; Xiao, P. F. Adsorption of Au(III), Pd(II), and Pt(IV) from aqueous solution onto graphene oxide. *J. Chem. Eng. Data* **2013**, *58*, 209−216.
(75) Liu, M. C.; Chen, C. L.; Hu, J.; Wu, X. L.; Wang, X. K. Synthesis of magnetite/graphene oxide composite and application for cobalt(II) removal. *J. Phys. Chem. C* **2011**, *115*, 25234−25240.
(76) Liu, L.; Li, C.; Bao, C. L.; Jia, Q.; Xiao, P. F.; Liu, X. T.; Zhang, Q. P. Preparation and characterization of chitosan/graphene oxide composites for the adsorption of Au(III) and Pd(II). *Talanta* **2012**, *93*, 350−357.
(77) Thakur, S.; Das, G.; Raul, P. K.; Karak, N. Green one-step approach to prepare sulfur/reduced graphene oxide nanohybrid for

effective mercury ions removal. *J. Phys. Chem. C* **2013**, *117*, 7636−7642.
(78) Li, Y. H.; Pan, Z.; Du, Q. J.; Peng, X. J.; Liu, T. H.; Wang, Z. H.; Xia, Y. Z.; Zhang, W.; Wang, K. L; Zhu, H. W.; Wu, D. H. Adsorption of fluoride from aqueous solution by graphene. *J. Colloid Interface Sci.* **2011**, *363*, 348−354.
(79) Tang, Y. L.; Guo, H. G.; Xiao, L.; Yu, S. L.; Gao, N. Y.; Wang, Y. L. Synthesis of reduced graphene oxide/magnetite composites and investigation of their adsorption performance of fluoroquinolone antibiotics. *Colloids Surf., A* **2013**, *424*, 74−80.